Turkish Journal of Electrical Engineering & Computer Sciences

http://journals.tubitak.gov.tr/elektrik/

Research Article

Turk J Elec Eng & Comp Sci
(2016) 24: 1279 – 1291

doi:10.3906/elk-1310-129

A discrete numerical method for magnetic field determination in three-phase busbars of a rectangular cross-section

Tomasz SZCZEGIELNIAK[1,*], Zygmunt PIATEK[1], Bernard BARON[2], PawełJABŁOŃSKI[1], Dariusz KUSIAK[1], Artur PASIERBEK[2]

[1]Environmental Engineering Institute, Czestochowa University of Technology, Czestochowa, Poland

[2]Institute of Theoretical and Industrial Electrical Engineering, Silesian University of Technology, Gliwice, Poland

Received: 20.10.2013 • **Accepted/Published Online:** 02.03.2014 • **Final Version:** 23.03.2016

Abstract: This paper presents a discrete numerical computation method for determining the magnetic field distributions in finite-length high-current bus ducts of rectangular busbars. This method is based on the integral equation method and the partial element equivalent circuit method. It takes into account the skin effect and proximity effects, as well as the complete electromagnetic coupling between phase bars and the neutral bar. In particular, the magnetic fields in busbars of unshielded three-phase systems with rectangular phase and neutral busbars and the use of the method are described. Finally, two applications to three-phase unshielded systems busbars are presented.

Key words: Rectangular busbar, high-current bus duct, magnetic field, numerical method

1. Introduction

High-current air-insulated bus duct systems with rectangular busbars are often used in power generation and substations due to their easy installation and utilization. The increasing power level of these plants requires an increase in the current-carrying capacity of the distribution lines (usually 1–10 kA). The medium voltage level of the generator terminals is 10–30 kV. The construction of the busbar is usually carried out by putting together several flat rectangular bars in parallel for each phase in order to reduce thermal stresses. The spacing between the bars is made equal to their thickness for practical reasons, and this leads to skin and proximity effects. The bus ducts usually consist of aluminum or copper busbars [1,2]. A typical cross-section of a shielded three-phase high-current bus duct is depicted in Figure 1.

Power busbars generate extremely low-frequency magnetic fields, which can cause disturbances in nearby computers and some other electrical, electronic, and digital devices. Power distribution three-phase busbar systems are one of the main sources of magnetic fields at industrial frequency and can generate electromagnetic interference by inductive coupling. Moreover, the presence of a low-frequency magnetic field generated by power busbars may produce some undesirable effects on human health [3–6]. Thus, a correct prediction of the magnetic field generated by high-current bus ducts is very important.

The distribution of AC magnetic fields in the region surrounding the busbars can be found exactly only for simple geometries like round wires and tubes [7], or very long and thin rectangular busbars (tapes or strips) [8–10]. For more complex cross-sections analytical-numerical and numerical methods must be used to find the magnetic field distributions, which is further modified by the proximity of other conductors, i.e. the "proximity

*Correspondence: szczegielniakt@interia.pl

effect" [4–6,11–15]. Both the skin effect and proximity effect will generally cause the magnetic field distribution to differ considerably from the expected one without taking into account both effects. The development of efficient numerical methods for the solutions of these problems is therefore of interest.

2. Multiconductor model of the busbars

In this model, each phase, neutral busbars, and each plate of the enclosure are divided into several thin subbars [2], as shown in Figure 2.

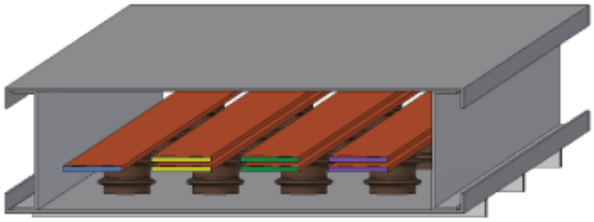

Figure 1. Three-phase high-current bus duct of rectangular cross-section with two busbars per phase and one neutral busbar (PELPO-Version II, manufactured by Elektrobudowa S.A., Katowice, Poland).

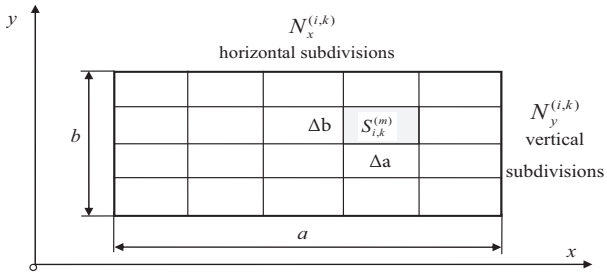

Figure 2. The kth bar of the ith phase divided into $N_{i,k} = N_x^{(i,k)} N_y^{(i,k)}$ subbars.

This division of the kth bar of the ith phase or the neutral into subbars is carried out separately for the horizontal (Ox axis) and vertical (Oy axis) direction of its cross-sectional area. Hence, subbars are generally rectangular in cross-section with width Δa and thickness Δb, defined by the following relations:

$$\Delta a = \frac{a}{N_x^{(i,k)}} \text{ and } \Delta b = \frac{b}{N_y^{(i,k)}}, \tag{1}$$

where a and $b$are the width and the thickness of the busbar, respectively, and $N_x^{(i,k)}$ and $N_y^{(i,k)}$ are the number of divisions along the busbar width and thickness, respectively. Thus, the total number of subbars of the kth bar of the ith phase is $N_{i,k} = N_x^{(i,k)} N_y^{(i,k)}$, and they are numbered by $m = 1, 2, \ldots, N_{i,k}$. For the lth bar of the jth phase or the neutral we have the total number of subbars $N^{j,l} = N_x^{(j,l)} N_y^{(j,l)}$ numbered by $n = 1, 2, \ldots, N^{j,l}$. All subbars have the same length l.

If the diagonal $[(\Delta a)^2 + (\Delta b)^2]^{1/2}$ of the mth subbar is small in comparison to the skin depth, we can neglect the skin effect and assume that the complex current density ($\mathrm{A/m^2}$) in the subbar can be considered uniform, i.e.

$$\underline{J}_{i,k}^{(m)} = \frac{\underline{I}_{i,k}^{(m)}}{S_{i,k}^{(m)}}, \tag{2}$$

where $\underline{I}_i^{(m,k)}$ is the complex current flowing through the mth subbar.

3. Current densities

For the mth subbar the integral equation can be written as follows [16]:

$$\frac{\underline{J}_{i,k}^{(m)}(X)}{\sigma_i} + \frac{j\omega\mu_0}{4\pi}\sum_{j=1}^{N_c}\sum_{l=1}^{N_j}\sum_{n=1}^{N_{j,l}}\int\limits_{v_{j,l}^{(n)}}\frac{\underline{J}_{j,l}^{(n)}(Y)}{\rho_{XY}}\,dv_{j,l}^{(n)} = \underline{u}_i, \tag{3}$$

where σ_i [S/m] is the electrical conductivity of ith phase bar, j is the imaginary unit, ω is the angular frequency of the currents, μ_0 [H/m] is the magnetic permeability of vacuum, u_i [V/m] is the voltage drop on the ith phase bar per unit of length, $v_j^{(n,l)}$ is the volume of the nth subbar or plate of the lth bar or plate of the jth phase or the neutral or the enclosure, and $\rho_{XY} = |X - Y|$ is the distance between the observation point $X = (x_1,\, y_1,\, z_1)$ and the source point $Y = (x_2,\, y_2,\, z_2)$.

Now we can divide Eq. (3) by the area $S_i^{(m,k)}$ and integrate over the volume $v_i^{(m,k)}$ of the mth subbar or plate, obtaining the following equation:

$$R_{i,k}^{(m)}\underline{I}_{i,k}^{(m)} + j\omega\sum_{j=1}^{N_c}\sum_{l=1}^{N_j}\sum_{n=1}^{N_{j,l}}M_{(i,k)(j,l)}^{(m,n)}\underline{I}_{j,l}^{(n)} = \underline{U}_i, \tag{4}$$

where $\underline{U}_i$ is the voltage drop across of all subbars of the ith phase or the neutral or the shield (they are connected in parallel), and the resistance of the mth subbar is defined by

$$R_{i,k}^{(m)} = \frac{l}{\sigma_i S_{i,k}^{(m)}}, \tag{5}$$

and the self or the mutual inductance is expressed as

$$M_{(i,k)(j,l)}^{(m,n)} = \frac{\mu_0}{4\pi\, S_{i,k}^{(m)}\, S_{j,l}^{(n)}}\int\limits_{v_{i,k}^{(m)}}\int\limits_{v_{j,l}^{(n)}}\frac{dv_{i,k}^{(m)}\, dv_{j,l}^{(n)}}{\rho_{XY}}. \tag{6}$$

The exact closed formulae for the self and the mutual inductance of a rectangular conductor of any dimensions, including any length, were given in [17] and [18], respectively. Not only do not we use the geometric mean distance here, we do not use the formula for mutual inductance between two filament wires, as well.

The set of equations like Eq. (4), written for all subbars, forms the following general system of complex linear algebraic equations:

$$\hat{\underline{U}} = \hat{\underline{Z}}\,\hat{\underline{I}}, \tag{7}$$

where $\hat{\underline{U}}$ and $\hat{\underline{I}}$ are column vectors of the voltages and currents of all subbars, respectively, and $\hat{\underline{Z}}$ is the symmetric matrix of self and mutual impedances (the impedance matrix) of all subbars, the elements of which are

$$\underline{Z}_{(i,k)(j,l)}^{(m.n)} = \begin{cases} R_{i,k}^{(m)} + j\omega\, M_{(i,k)(j,l)}^{(m,n)} & m = n,\ i = j,\ k = l, \\ j\omega\, M_{(i,k)(j,l)}^{(m,n)} & \text{otherwise.} \end{cases} \tag{8}$$

We can then find the admittance matrix $\hat{\underline{Y}}$, which is the inverse matrix of the impedance matrix $\hat{\underline{Z}}$, and it is expressed as

$$\hat{\underline{Y}} = \left[\underline{Y}^{(m,n)}_{(i,k)(j,l)}\right] = \hat{\underline{Z}}^{-1} \tag{9}$$

and has a similar structure as $\hat{\underline{Z}}$. It is then possible to determine the current of the mth subbar of the kth bar of the ith phase or the neutral as

$$\underline{I}^{(m)}_{i,k} = \sum_{j=1}^{N_c} \sum_{l=1}^{N_j} \sum_{n=1}^{N_{j,l}} \underline{Y}^{(m,n)}_{(i,k)(j,l)} \underline{U}_j. \tag{10}$$

The total current of the ith phase or the neutral is

$$\underline{I}_i = \sum_{k=1}^{N_i} \sum_{m=1}^{N_{i,k}} \underline{I}^{(m)}_{i,k}. \tag{11}$$

By inserting Eq. (12) into Eq. (13), we obtain

$$\underline{I}_i = \sum_{j=1}^{N_c} \underline{Y}\underline{U}_j, \tag{12}$$

where

$$\underline{Y} = \sum_{k=1}^{N_i} \sum_{m=1}^{N_{i,k}} \sum_{l=1}^{N_j} \sum_{n=1}^{N_{j,l}} \underline{Y}^{(m,n)}_{(i,k)(j,l)}. \tag{13}$$

From the admittance matrix with elements given by Eq. (13), we can determine the impedance matrix of shielded three-phase system busbars with the neutral busbar as follows:

$$\underline{Z} = [\underline{Z}] = \underline{Y}^{-1} = [\underline{Y}]^{-1}. \tag{14}$$

The impedances $\underline{Z}_{i,j}$ in Eq. (14), which are obtained from Eqs. (5), (6), (8), (9), and (13), comprise information related only to construction and material, whereas their values are not affected by the busbar currents but only by their cross-sectional distribution. Therefore, the skin and proximity effects are taken into consideration.

If we assume all sinusoidal phase currents to be given, we can write that the neutral current $\underline{I}_N = \underline{I}_1 + \underline{I}_2 + \underline{I}_3$ and, from Eq. (12), find all voltages across phase and neutral busbars as

$$\underline{U}_i = \sum_{j=1}^{N_c} \underline{Z}\underline{I}_j. \tag{15}$$

From that and Eq. (12) it is possible to determine all currents in subbars and finally calculate, according to Eq. (4), the current densities in them. These densities differ in the cross-sections of the busbars due to the skin and proximity effects.

4. Magnetic field

Knowing the current from Eq. (10) in each subbar, evaluation of the magnetic field can be performed. The vector magnetic potential $\underline{\boldsymbol{A}}_i^{(m,k)}(X)$, in Wb/m, induced by the mth subbar (Figure 3), is given by

$$\underline{A}_{i,k}^{(m)}(X) = \frac{\mu_0}{4\pi} \iiint\limits_{v_{i,k}^{(m)}} \frac{\underline{J}_{i,k}^{(m)}(Y)}{\rho_{XY}} dv = \mathbf{a}_z \underline{A}_{i,k}^{(m)}(x,y,z), \tag{16}$$

where $X = (x,\ y,\ z)$, $Y = (x_1,\ y_1,\ z_1)$, and $\rho_{XY} = |X - Y|$.

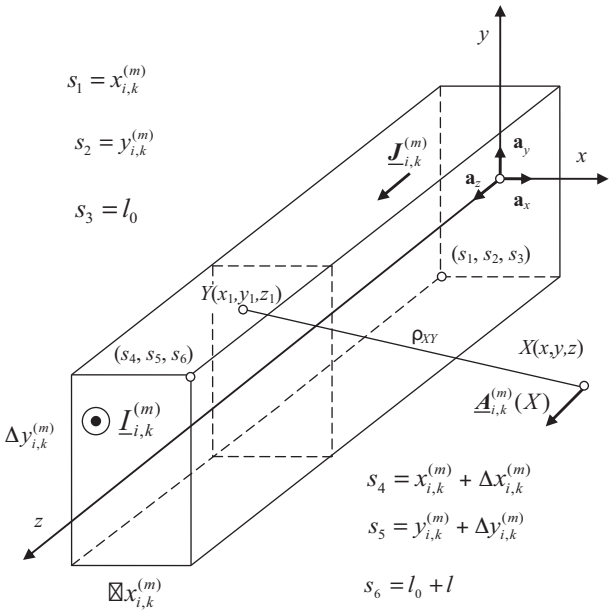

Figure 3. The mth subbar of the kth bar of the ith phase with the current $\underline{I}_i^{(m,k)}$, which generates the vector magnetic potential $\underline{\boldsymbol{A}}_i^{(m,k)}$ at point X.

If $l >> \Delta x_i^{(m,k)}$ and $l >> \Delta y_i^{(m,k)}$ as well as $|x - x_1| >> \Delta x_i^{(m,k)}$ and $|y - y_1| >> \Delta y_i^{(m,k)}$, the integral of Eq. (16) can be rewritten as

$$\underline{A}_{i,k}^{(m)}(x,y,z) = \frac{\mu_0 \underline{I}_{i,k}^{(m)}}{4\pi} \int\limits_{l_0}^{l_0+l} \frac{dz_1}{\rho_{XY}^{(m)}}, \tag{17}$$

where

$$\begin{aligned} \rho_{XY}^{(m)} \quad = \quad & \sqrt{(x - x_{i,k}^{(m)} - \tfrac{1}{2}\Delta x_{i,k}^{(m)})^2 + } \\ & + \overline{(y - y_{i,k}^{(m)} - \tfrac{1}{2}\Delta y_{i,k}^{(m)})^2 + (z - z_1)^2}. \end{aligned} \tag{18}$$

Hence, the complex magnetic field strength (in A/m) has two components only, which are given by

$$\underline{H}_{x,i,k}^{(m)}(X) = -\frac{\underline{I}_{i,k}^{(m)}}{4\pi} \int\limits_{l_0}^{l_0+l} \frac{(y - y_{i,k}^{(m)} - \frac{1}{2}\Delta y_{i,k}^{(m)})}{(\rho_{XY}^{(m)})^3} dz_1 \tag{19}$$

and

$$\underline{H}_{y,i,k}^{(m)}(X) = \frac{\underline{I}_{i,k}^{(m)}}{4\pi} \int_{l_0}^{l_0+l} \frac{(x - x_{i,k}^{(m)} - \frac{1}{2}\Delta x_{i,k}^{(m)})}{(\rho_{XY}^{(m)})^3} dz_1. \tag{20}$$

The integrals in Eqs. (19) and (20) are the standard integrals whose solutions are well known, i.e. we have that

$$\Im(z, a, b) = \int \frac{b\, d\xi}{[a^2 + b^2 + \xi^2]^{3/2}} = \frac{b}{a^2 + b^2} \frac{\xi}{\sqrt{a^2 + b^2 + \xi^2}} \tag{21}$$

for $\xi = z - z_1$. Thus, assuming $l_0 = 0$, the components of the magnetic field can be rewritten as

$$\underline{H}_{x,i,k}^{(m)}(X) = \frac{\underline{I}_{i,k}^{(m)}}{4\pi} \left[\begin{array}{l} \Im(z, x - x_{i,k}^{(m)} - \frac{1}{2}\Delta x_{i,k}^{(m)}, y - y_{i,k}^{(m)} - \frac{1}{2}\Delta y_{i,k}^{(m)}) \\ -\Im(l - z, x - x_{i,k}^{(m)} - \frac{1}{2}\Delta x_{i,k}^{(m)}, y - y_{i,k}^{(m)} - \frac{1}{2}\Delta y_{i,k}^{(m)}) \end{array} \right] \tag{22}$$

and

$$\underline{H}_{y,i,k}^{(m)}(X) = -\frac{\underline{I}_{i,k}^{(m)}}{4\pi} \left[\begin{array}{l} \Im(z, y - y_{i,k}^{(m)} - \frac{1}{2}\Delta y_{i,k}^{(m)}, x - x_{i,k}^{(m)} - \frac{1}{2}\Delta x_{i,k}^{(m)}) \\ -\Im(l - z, y - y_{i,k}^{(m)} - \frac{1}{2}\Delta y_{i,k}^{(m)}, x - x_{i,k}^{(m)} - \frac{1}{2}\Delta x_{i,k}^{(m)}) \end{array} \right]. \tag{23}$$

The total magnetic field is given by

$$\underline{H}_x(X) = \sum_{i=1}^{N_c} \sum_{k=1}^{N_i} \sum_{m=1}^{N_{i,k}} \underline{H}_{x,i,k}^{(m)}(X) \tag{24}$$

and

$$\underline{H}_y(X) = \sum_{i=1}^{N_c} \sum_{k=1}^{N_i} \sum_{m=1}^{N_{i,k}} \underline{H}_{y,i,k}^{(m)}(X). \tag{25}$$

In three-phase busbar systems, the magnetic field is elliptical [19]. Its instantaneous value equals

$$\mathbf{H}(X, t) = a_x \sqrt{2} Re(\underline{H}_x e^{j\omega t}) + a_y \sqrt{2} Re(\underline{H}_y e^{j\omega t}) \tag{26}$$

and its major and minor RMS values, respectively, can be found as follows:

$$H_{\max}(X) = \max_{0 \le t \le T} \frac{|H(X, t)|}{\sqrt{2}} = |\underline{H}_1(X)| + |\underline{H}_2(X)|, \tag{27}$$

$$H_{\min}(X) = \min_{0 \le t \le T} \frac{|H(X, t)|}{\sqrt{2}} = ||\underline{H}_1(X)| - |\underline{H}_2(X)||, \tag{28}$$

where

$$\underline{H}_1(X) = \frac{\underline{H}_x(X) + j\, \underline{H}_y(X)}{2}, \tag{29}$$

$$\underline{H}_1(X) = \frac{\underline{H}_x^*(X) + j\, \underline{H}_y^*(X)}{2}. \tag{30}$$

5. Numerical examples

The first numerical example selected for this paper features a three-phase system of rectangular busbars with one neutral busbar, whose cross-section is depicted in Figure 4. According to the notations applied in this figure, the following geometry of the busbars has been selected: the dimensions of the phase rectangular busbars and the neutral busbars are $a = 60$ mm, $b = b_1 = 5$ mm, $d = d_1 = 90$ mm. The phase busbars and the neutral are made of copper, which has the electric conductivity of $\sigma = 56$ MS m^{-1}. The frequency is 50 Hz. All phases have two busbars per phase – $N_1 = N_2 = N_3 = 2$, and the neutral has one busbar – $N_4 = 1$. The length of the busbar system is assumed to be $l = 10$ m. In the numerical procedure, each phase busbar is divided into $N_x^{(i,k)} = 30$ and $N_y^{(i,k)} = 5$, which gives 150 subbars for each busbar. Hence, all three phases and the neutral busbars have 1050 subbars in total. With the chosen division, each rectangular subbar has dimensions of 2×1 mm. This allows for the fact that the current density is uniform on the surface of the subbars. During the simulation, three balanced currents with busbar-rated values $I_1 = 1$ kA are imposed in phases as shown:

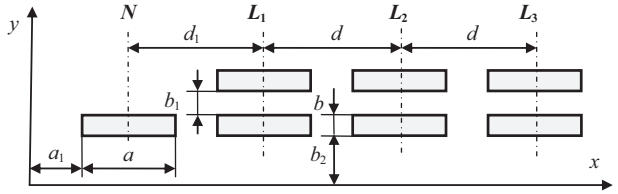

Figure 4. Three-phase high-current bus duct of rectangular cross-section with two busbars per phase and one neutral busbar.

$$\underline{I}_2 = \underline{I}_1 e^{-j120^o}, \qquad \underline{I}_3 = \underline{I}_1 e^{j120^o}, \; and \; \underline{I}_N = \underline{I}_1 + \underline{I}_2 + \underline{I}_3 = 0. \tag{31}$$

As a first result, the current density comparison along the x axis, practically the same along y axis at $x = \text{const}$, in each busbar is shown in Figure 5.

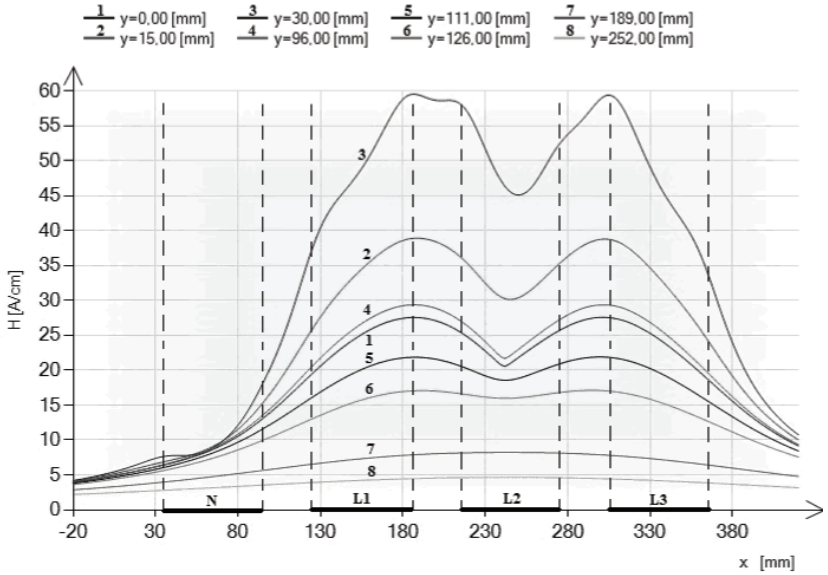

Figure 5. Magnetic field $H_{\max}$ (RMS value) against x at different heights in the high-current three-phase bus ducts with two busbars per phase and one neutral bar in the case of three balanced currents ($a_1 = 35$ mm, $b_2 = 45$ mm; see Figure 4).

The case of three unbalanced currents,

$$\underline{I}_2 = 0.5\underline{I}_1 e^{-j120^o},\ \ \underline{I}_3 = \underline{I}_1 e^{j120^o} and\ \ \underline{I}_N = \underline{I}_1 + \underline{I}_2 + \underline{I}_3 = 0.5\, e^{j60^o}, \tag{32}$$

has been also investigated (Figure 6).

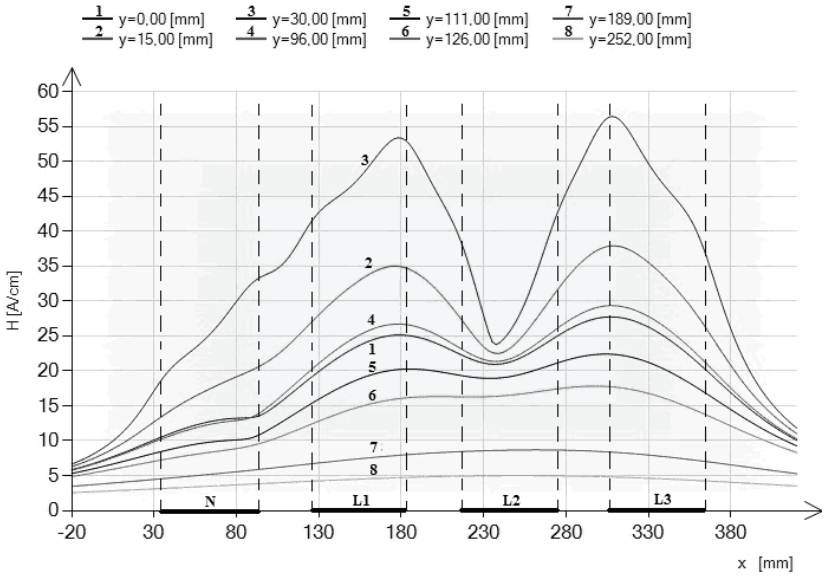

Figure 6. Magnetic field $H_{\max}$ (RMS value) against x at different heights in the high-current three-phase bus ducts with two busbars per phase and one neutral bar in the case of three unbalanced currents ($a_1 = 35$ mm, $b_2 = 45$ mm; see Figure 4).

The second configuration of a three-phase busbar system, the current density of which is investigated, is shown in Figure 7. It has only one busbar per phase and neutral – $N_1 = N_2 = N_3 = N_4 = 1$. The length of the busbar system and the busbar division are as in the previous example (150 subbars for each busbar). Hence, all three-phase and neutral busbars have 600 total subbars. With the chosen division, each rectangular subbar still has dimensions of 2 × 1 mm. During the simulation, three balanced – Eq. (31) – and three unbalanced – Eq. (32) – currents with busbar-rated values $I_{eff} = 1$ kA are imposed in phases, and the comparison of current densities along the x axis, practically the same along the y axis at $x = \text{const.}$, in each busbar is shown in Figure 8 and Figure 9, respectively.

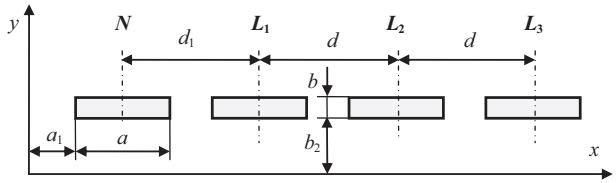

Figure 7. Three-phase high-current bus duct of rectangular cross-section with one busbar per phase and one neutral busbar.

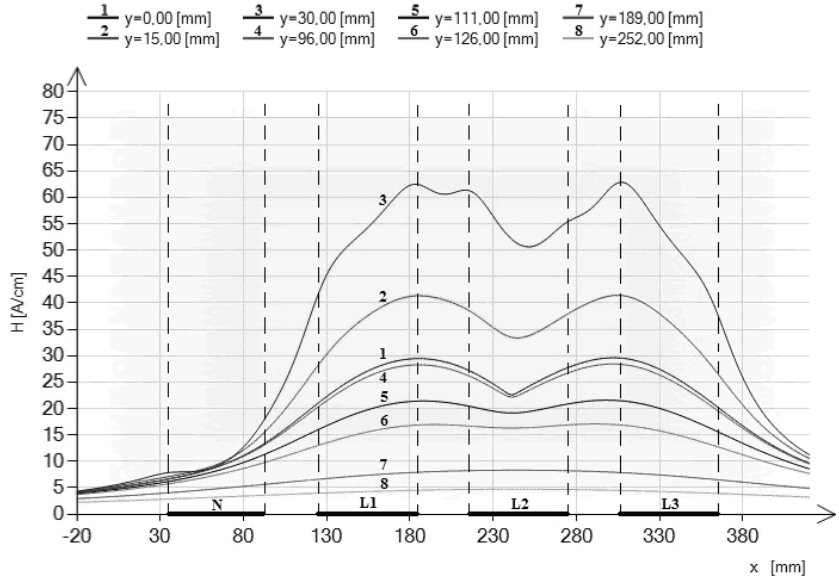

Figure 8. Magnetic field $H_{\max}$ (RMS value) against x at different heights in the high-current three-phase bus ducts with one busbar per phase and one neutral bar in the case of three balanced currents ($a_1 = 35$ mm, $b_2 = 45$ mm; see Figure 7).

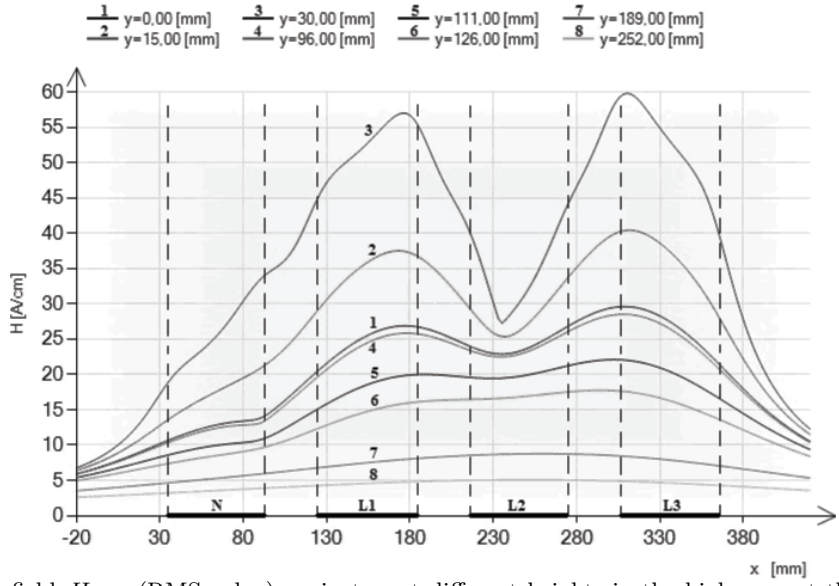

Figure 9. Magnetic field $H_{\max}$ (RMS value) against x at different heights in the high-current three-phase bus ducts with one busbar per phase and one neutral bar in the case of three unbalanced currents ($a_1 = 35$ mm, $b_2 = 45$ mm; see Figure 7).

6. Comparison of results

To verify the computed magnetic field, we also carried out suitable measurements. Magnetic fields of the busbars systems were measured in the laboratory on an experimental setup (Figure 10). In the measurements, a three-phase current of 1000 A was injected into a test system by a special AC current source. The experiments were

performed under a 50 Hz sinusoidal supply. The busbars systems under test were 3.9 m long and terminated at one end by a short connector. The results of the measurements and calculations are shown in Tables 1 and 2.

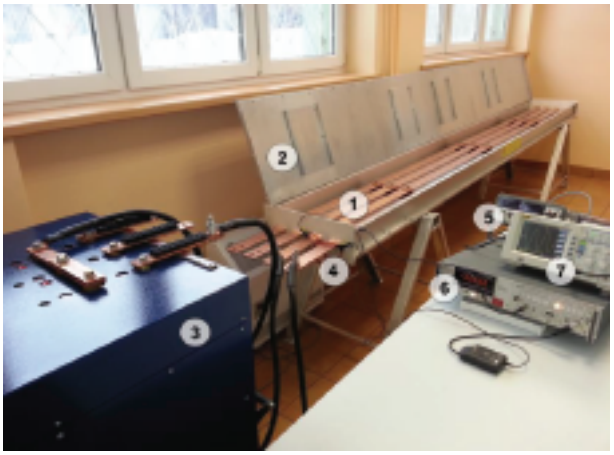

Figure 10. Laboratory stand for magnetic field measurements in three-phase busbar system, 1 – busbars, 2 – enclosure (open top cover), 3 – supply, 4 – Rogowski coil, 5 – digital voltmeter, 6 – digital phase meter, 7 – oscilloscope.

Table 1. Magnetic field in kA/m of three-phase high-current bus ducts of rectangular cross-section with a neutral busbar depicted in Figure 13.

Method		Points											
		1	2	3	4	5	6	7	8	9	10	11	12
*	IEM	0.385	0.950	6.450	7.850	6.650	0.985	0.450	0.855	1.860	2.145	1.885	0.750
	FEM	0.504	1.288	8.034	8.100	7.791	1.213	0.441	1.013	2.106	2.487	2.091	0.898
	MM	0.449	1.113	5.927	6.366	5.918	1.097	0.457	0.934	1.792	2.321	1.800	0.793
**	IEM	0.565	1.645	6.450	3.565	6.255	0.995	0.450	0.985	1.865	2.065	1.960	0.785
	FEM	0.457	1.812	7.985	4.761	7.910	1.306	0.416	1.004	2.050	2.318	2.151	0.961
	MM	0.416	1.463	6.157	3.621	6.278	1.128	0.384	0.913	1.694	2.179	1.850	0.766

* - Balanced currents.
** - Unbalanced currents.
IEM - Integral equation method.
FEM - FEMM computations.
MM - Measurements.

The measurement system is presented in Figure 11. The fundamental element of the measurement system is the magnetic field sensor (Figure 12), which is connected with a computer by means of optical fiber and a converter. Output voltages of the sensor are functions of the measured magnetic field components. The magnetic field in the three-phase high-current bus ducts was measured at the points shown in Figures 13 and 14.

Apart from numerical calculation, computer simulations for the three-phase unshielded busbars system were also performed with the aid of the commercial FEMM software [20], using two-dimensional finite elements. Figure 15 shows the computational finite element mesh for three-phase busbars.

From Tables 1 and 2 it follows that the measured values of the magnetic field are very close to the computed ones with the use of the integral equation method. In general, the relative error does not exceed 10% for balanced and unbalanced currents. It is noticeable that the measured values are slightly larger than the computed ones, especially for the high-current bus duct with one busbar per phase. The increased values

probably come from uncertainty of some parameter values that are included in the computational model, such as the conductivity of copper. The laboratory high-current bus duct probably has slightly different physical parameters than those given by the producer.

Table 2. Magnetic field in kA/m of three-phase high-current bus ducts of rectangular cross-section with a neutral busbar depicted in Figure 14.

Method		Points											
		1	2	3	4	5	6	7	8	9	10	11	12
*	IEM	0.375	0.915	5.120	6.265	6.250	0.955	0.365	0.750	1.890	1.980	1.650	0.665
	FEM	0.518	1.323	7.409	7.813	7.293	1.251	0.449	1.009	2.020	2.417	2.014	0.903
	MM	0.460	1.078	5.765	5.955	6.154	0.991	0.346	0.843	1.701	2.137	1.902	0.716
**	IEM	0.525	1.655	6.885	4.785	6.825	0.985	0.385	0.950	1.780	2.155	2.000	0.750
	FEM	0.460	1.888	7.293	5.116	7.317	1.332	0.413	0.975	1.937	2.264	2.055	0.956
	MM	0.486	1.476	5.528	3.921	6.129	0.987	0.320	0.885	1.636	1.922	1.930	0.727

* - Balanced currents.
** - Unbalanced currents.
IEM - Integral equation method.
FEM - FEMM computations.
MM - Measurements.

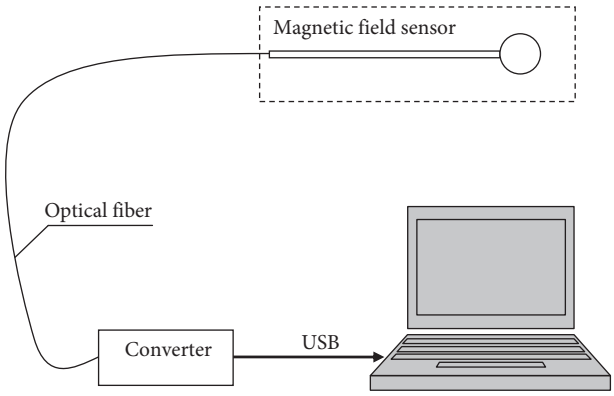

Figure 11. Block diagram of the measurement system.

Figure 12. Magnetic field sensor.

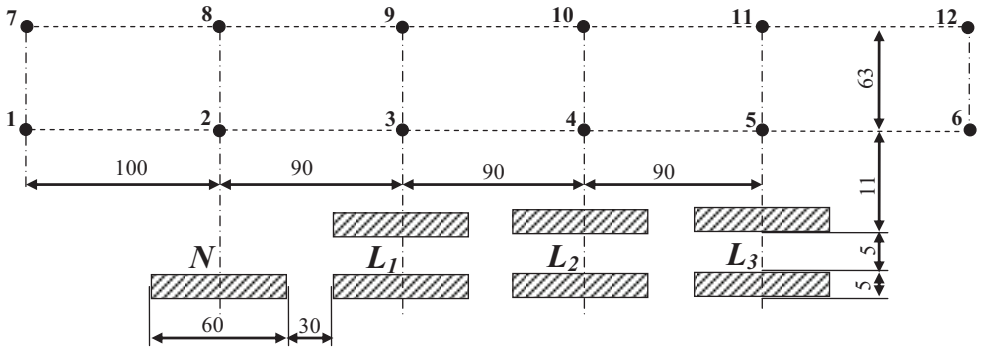

Figure 13. Measurement points for the three-phase high-current bus duct with two busbars per phase.

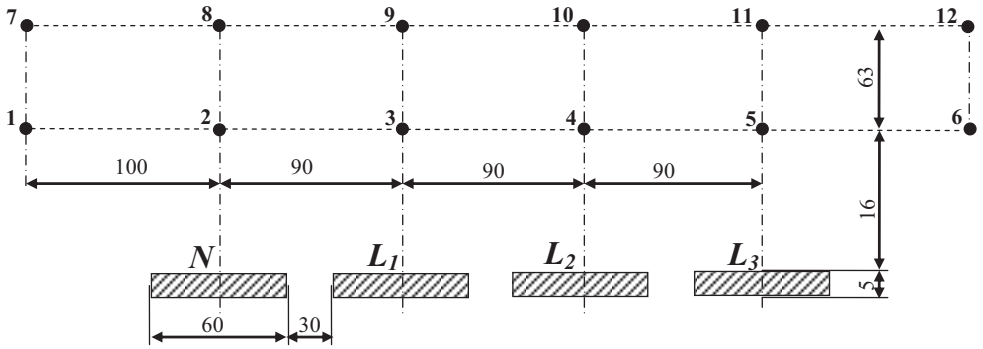

Figure 14. Measurement points for the three-phase high-current bus duct with one busbar per phase.

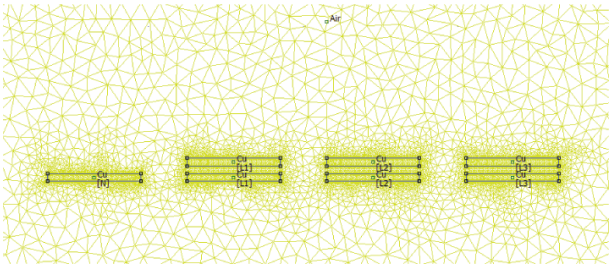

Figure 15. The finite element mesh used in FEMM computations.

The discrepancies between measured values and FEMM computations are caused by the calculation methods. In the integral equation method, the authors used Eq. (27) to obtain the maximum value of the magnetic field, but FEMM software uses the following formula:

$$\|H\| = \sqrt{\underline{H}_x \underline{H}_x^* + \underline{H}_y \underline{H}_y^*}. \tag{33}$$

Besides, FEMM performs 2D field computations, whereas our method uses the formulae for finite-length conductors.

7. Conclusions

A finite-length approach to the solution of the magnetic field distribution in the high-current bus ducts of a rectangular cross-section has been presented in this paper. The proposed approached combines the partial element equivalent circuit method with the exact closed formulae for AC self and mutual inductances of rectangular conductors of any dimensions, which allows precise accounting for the skin and proximity effects. Complete electromagnetic coupling between the phase busbars and the neutral busbar is taken into account, as well.

As Figures 5 and 6 as well as 8 and 9 show, both the skin effect and the proximity effect will generally cause the magnetic field distribution to differ considerably from the expected one without taking into account both effects, especially very near the busbars. Knowing the magnetic field and current distribution, the evaluation of the electrodynamic force on each busbar can be performed.

The proposed method allows us to calculate the magnetic field intensity distribution in a set of parallel rectangular busbars of any dimensions, including any length. The model is strikingly simple, and from a logical standpoint it can be applied in general to conductors of any cross-section, whereas many conventional methods, being much more complicated, often require a greater or lesser degree of symmetry. From the practical

standpoint of the calculations involved, the model requires the solution of a rather large set of linear simultaneous equations. However, this solution is well within the range of the ability of existing computers, even those that are somewhat older.

References

[1] Ducluzaux A. Extra Losses Caused in High Current Conductors by Skin and Proximity Effects. Schneider Electric Cahier Technique No. 83. Rueil-Malmaison, France: Schneider Electric, 1983.

[2] Sarajčev P, Goič R. Power loss computation in high-current generator bus ducts of rectangular cross-section. Electr Pow Compo Sys 2010; 39: 1469-1485.

[3] Keikko T, Korpinen L, Partanen J. Calculation of magnetic fields of the bus bar. In: UPEC'95 30th Universities Power Engineering Conference; 5–7 September 1995; Greenwich, UK. London, UK: University of Greenwich. pp. 554-557.

[4] Cucu M, Popescu MO. Magnetic field in encapsulated bus-bar. UPB Sci Bull C 2011; 73: 129-142.

[5] Sha X, Xianlong J, Feng P, Jie S. Analysis of 3-D electromagnetic field for three-phase low voltage and heavy current busbar bridge system. Int J Appl Electromagn Mech 2007; 26: 37-49.

[6] Bottausio O, Carpaneto E, Chiampi M, Chiarabaglio D, Panaitescu I. Numerical and experimental evaluation of magnetic field generated by power busbar systems. IEE P-Gener Transm D 1996; 143: 455-460.

[7] Piątek Z. Impedances of Tubular High Current Busducts. Warsaw, Poland: Polish Academy of Sciences, 2008.

[8] Zhou J, Lewis AM. Thin-skin electromagnetic fields around a rectangular conductor bar. J Phys D Appl Phys 1994; 27: 419-425.

[9] Kazimierczuk MK. High-Frequency Magnetic Components. Chichester, UK: Wiley & Sons, 2009.

[10] Abdelbagi HA. Skin and proximity effect in two parallel plates. MSc, Wright State University, Dayton, OH, USA, 2007.

[11] Sarajčev P. Numerical analysis of the magnetic field of high-current busducts and GIL systems. Energies 2011; 4: 2196-2211.

[12] Canova A, Giaccone L. Numerical and analytical modeling of busbar systems. IEEE T Power Deliver 2009; 24: 1568-1577.

[13] Bourmanne P, Delince F, Genon A, Legros W, Nicolet A. Skin effect and proximity effect in multiconductor systems with applied currents and voltages. J Appl Phys 1991; 69: 5035-5037.

[14] Greconici M, Madescu G, Mot M. Skin effect in a free space conductor. Facta Universitatis (Niš) Ser Elec Energ 2010; 23: 207-215.

[15] Jafari-Shapoorabadi R, Konrad A, Sinclair AN. Comparison of three formulations for eddy-current and skin effect problems. IEEE T Magn 2002; 38: 617-620.

[16] Piątek Z, Baron B, Szczegielniak T, Kusiak D, Pasierbek A. Numerical method of computing impedances of a three-phase busbar system of rectangular cross section. Prz Elektrotechniczn 2013; 7: 150-154.

[17] Piątek Z, Baron B. Exact closed form formula for self inductance of conductor of rectangular cross section. Prog Electromagn Res M 2012; 26: 225-236.

[18] Piątek Z, Baron B, Szczegielniak T, Kusiak D, Pasierbek A. Exact closed form formula for mutual inductance of conductors of rectangular cross section. Prz Elektrotechniczn 2013; 3a: 61-64.

[19] Piątek Z, Szczegielniak T, Kusiak D. Elliptical magnetic field in high-current busducts. Prz Elektrotechniczn 2010; 4: 101-106 (in Polish with abstract in English).

[20] Meeker DC. Finite Element Method Magnetics, Version 4.2, User's Manual. Available online at http://www.femm.info/Archives/doc/manual42.pdf.